On the Structure of Water at the Aqueous/Air Interface

Yubo Fan, Xin Chen, Lijiang Yang, Paul S. Cremer,* and Yi Qin Gao*

Department of Chemistry, Texas A&M University, College Station, Texas 77843

Received: January 6, 2009; Revised Manuscript Received: July 2, 2009

Vibrational sum frequency spectroscopy (VSFS) and molecular dynamics (MD) simulations were used in concert to investigate the molecular structure and hydrogen bonding of the air/water interface. MD simulations were performed with a variety of water models. The results indicated that only the upper most two layers of water molecules are ordered in this system. There is a strong preference to have the top layer arranged such that the OH moiety points upward into the air. This orientational preference arises from two factors that involve the maximization of the number of hydrogen bonds formed and the minimization of partial charge that is exposed. Specifically, the lone pairs from oxygen are less likely to face into the air compared with the OH moiety because this would expose more partial charge and, therefore, be unfavorable on enthalpic grounds. The two-layer interfacial water structure model implies that there should be four distinct types of OH stretches for this system. Namely, one directs upward and another points downward in each layer. Interestingly, VSFS experiments revealed the presence of four OH stretch region peaks at 3117, 3222, 3448, and 3696 cm^{-1}. The phases of the 3117 and 3696 cm^{-1} resonances carried a positive sign, which indicates that these features arise from OH groups with protons facing upward toward the air. The other two resonances emanate from OH groups with protons facing downward toward the bulk aqueous solution. On the basis of this, we assign the 3117 cm^{-1} peak to the OH moiety from a water molecule in the second layer, which is hydrogen bonded upward toward the top layer. On the other hand, the peak at 3222 cm^{-1} should arise from water molecules in the top layer with the OH moiety facing downward to hydrogen bond to the second layer. The 3448 cm^{-1} peak arises from hydrogen bonding between water molecules in the second layer and the more disordered water molecules of the bulk liquid. Finally, the peak at 3696 cm^{-1} is assigned to the free OH moiety pointing upward in the top layer.

Introduction

Interfacial water plays a key role in chemistry, physics, and biology.[1–3] Significant progress has been made in recent years in understanding the microscopic properties of aqueous surfaces due to extensive experimental and theoretical efforts. For example, powerful optical techniques, such as vibrational sum-frequency spectroscopy (VSFS), have been employed to characterize the OH stretch range of water molecules that are organized at interfaces.[1,4–6] Due to its quantum mechanical selection rules, VSFS is intrinsically surface-specific and has proven to be particularly useful at providing the molecular level details of the air/water interface. Three pronounced features have been observed in the VSF spectrum, which include a sharp peak at ~3700 cm^{-1} that has been assigned to a dangling OH bond, a broad feature near 3200 cm^{-1}, and a second broad feature centered at about 3450 cm^{-1}. Recently, Shen and co-workers employed phase-sensitive VSFS to identify the values of the real and imaginary components of the nonlinear susceptibility, $\chi^{(2)}$, for the OH stretch range as a function of frequency.[7] It was found that the imaginary component of $\chi^{(2)}$ changes sign twice between 3000 and 3800 cm^{-1}. In particular, positive amplitude is associated with the 3700 cm^{-1} peak, but the sign becomes negative in the region approximately from 3200 to 3600 cm^{-1}. Finally, the sign returns to a positive value below 3200 cm^{-1}. Earlier calculations produced simulated VSFS spectra that are only partially consistent with these new

experimental results. Specifically, agreement is generally found above 3200 cm^{-1}, but not below this value.[8,9]

In addition to experimental studies, molecular dynamics simulations using a number of different empirical water models have found that the HOH plane tends to be perpendicular to the plane of the air/water surface with one OH bond pointing out of the surface.[2,10–14] Ab initio molecular dynamics simulations have also been performed on water clusters.[11,15] These studies have provided evidence for interfacial water molecules with a single dangling OH bond ("single-donor" water), in agreement with VSFS experiments. In some cases, however, they have also found evidence for "acceptor-only" water species with two dangling OH bonds. This latter observation would be most consistent with early X-ray absorption spectroscopy studies,[16,17] although more recent ones favor the "single-donor" model.[18]

In the present study, we have revisited the problem of interfacial water structure with a combined experimental and computational approach. Extensive molecular dynamics simulations were performed using a variety of different water models. The aim of this work was to develop a simple molecular level picture that could be related to the VSFS results. The findings of the present investigations show that there are four major VSFS resonances in the OH stretch region. These peaks correspond to four chemically distinct OH moieties in the top two water layers at the interface (Scheme 1). Specifically, the free OH moieties in the top layer pointing into the air give rise to the VSFS peak at 3696 cm^{-1}. The OH bonds pointing downward from the same water molecules yield the resonance at 3222 cm^{-1}. The OH groups pointing upward from the waters

Structure of Water at the Aqueous/Air Interface

J. Phys. Chem. B, Vol. 113, No. 34, 2009 **11673**

SCHEME 1: A Schematic Representation of the Structure and Hydrogen Bonding of the Air/Water Interface
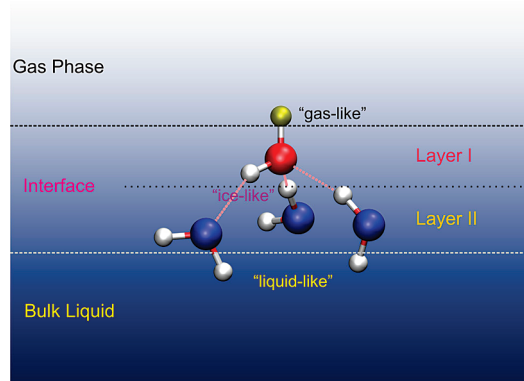
in the second layer are associated with the peak at 3117 cm^{-1}. Finally, the OH groups pointing downward from the waters in the second layer are responsible for the feature at 3448 cm^{-1}.

Methods

Molecular Dynamics Simulations. In the present study, several water models, including SPC/E,[19] TIP3P,[20,21] TIP4P-Ew,[22] TIP5P[21] and POL3,[23] were employed to simulate the molecular structure of the air/water interface. The relevant parameters for these models are provided in Table 1. A modified TIP5P model (mTIP5P) with T_d symmetry was also included to investigate the charge−charge interactions between protons and electron lone pairs (extra points in TIP5P) in a water molecule. In this system the protons and the negative charges occupy the apexes of a perfect tetrahedron, while oxygen sits at the center and the distance from the charges to the oxygen is 0.85 Å. All calculations were carried out with the AMBER 9 suite of programs.[24] A cuboid box was created with 8049 water molecules evenly filled in the initial configuration (Scheme 2). The systems were further extended by using periodic boundary condition. The SHAKE algorithm[25] was used to constrain all bonds involving hydrogens. A cutoff of 10.0 Å was applied for nonbonding interactions. The particle mesh Ewald method was applied to treat long-range electrostatic interactions.[26]

To obtain a reasonable initial structure, an *NPT* (number, pressure, temperature) ensemble calculation was performed. To do this, a 20-ps MD simulation was first conducted to heat the system from 0 to 360 K, followed by a 200-ps equilibration at 360 K and 1 atm. Next, the system was cooled to 300 K by another 20-ps MD simulation followed by a 1-ns equilibration at 300 K and 1 atm. The resulting final box size was approximately 40 × 40 × 155 Å^3.

In a second step, the *z* dimension was increased to 300 Å while the *x* and *y* dimensions were kept intact, resulting in a column geometry containing two air/water interfaces (Scheme 2). Starting from the configuration obtained from the last frame of the NPT calculation, the system was reheated from 0 to 360 K in a 20-ps *NVT* (number, volume, temperature) MD simulation followed by a 200-ps equilibration before it was cooled down to 300 K in another 20-ps MD simulation. The system was again equilibrated for 1 ns before 10- or 20-ns data collection runs were performed at 0.5-ps intervals. All the computations in this part were carried out under the *NVT* ensemble.

As shown in Scheme 2, the orientation of the O−H bond, the O-Lp (lone pair), and the water dipole were defined by the

angles between these vectors and the *z* axis (labeled as θ_H, θ_n, and θ_d, respectively). For those water models without lone pairs, such as SPC/E, TIP3P, and TIP4P-Ew, virtual lone pairs were created to occupy two of the apexes of a tetrahedron with the oxygen atom at the center and the hydrogen atoms positioned at the other two apexes.

Vibrational Sum-Frequency Spectroscopy (VSFS). VSFS measurements were performed as described previously.[27,28] The laser source was a passive-active mode-locked Nd:YAG laser (PY61c, Continuum, Santa Clara, CA) containing a negative feedback loop. The IR and visible beams were generated with an optical parametric generator/oscillator stage (LaserVision, Bellevue, WA). The visible beam was kept at 532 nm, while the IR beam was tuned from 2800 to 3800 cm^{-1}. The laser beams were combined spatially and temporally at the air/water interface. The visible beam was reflected off the water surface at an angle of 42° with respect to the surface normal. The IR was reflected at an angle of 51°. VSF spectra were taken with the ssp polarization combination. This notion refers to the polarization of the sum frequency, visible, and infrared beams, respectively. The spectra were normalized against a piece of Y-cut crystalline quartz and fit according to standard methods as previously reported.[1,5,27] Briefly, the intensity of the sum frequency signal, I_{SFG}, follows eq 1

$$I_{SFG} \propto |\chi_{eff}^{(2)}|^2 I_{vis} I_{IR} \tag{1}$$

where I_{vis} and I_{IR} are the intensities of the incoming visible and infrared laser beams, respectively. The effective second-order nonlinear susceptibility, $\chi_{eff}^{(2)}$, can be written as

$$\chi_{eff}^{(2)} = \chi_{NR}^{(2)} + \chi_{R}^{(2)} = \chi_{NR}^{(2)} + \sum_q \frac{A_q}{\omega_{IR} - \omega_q + i\Gamma_q} \tag{2}$$
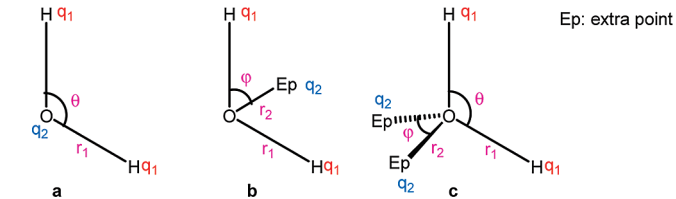
where $\chi_{NR}^{(2)}$ and $\chi_{R}^{(2)}$ are the frequency-independent nonresonant term and the frequency-dependent resonant term, respectively. $\chi_{R}^{(2)}$ of the *q*th resonant mode is a function of the oscillator strength, A_q; resonant frequency, ω_q; peak width, Γ_q; and the frequency of the input infrared laser beam, ω_{IR}.

Results

VSFS. Figure 1a shows the vibrational sum frequency spectrum of the OH stretch region at the air/water interface. The overall fit to the experimental data is given by a solid red line. The individual peaks and their corresponding signs are abstracted from this fitting (Figure 1b). The methods employed to fit the data have been previously reported.[1,5,27] Moreover, the abstracted parameters are provided in Table 1. There are four peaks: a sharp resonance at 3696 cm^{-1} and three very broad features at 3448, 3222, and 3117 cm^{-1}, respectively. These peaks can be categorized into two groups: non-hydrogen-bonded and hydrogen-bonded OH stretches. The 3696 cm^{-1} peak, which has a frequency very similar to gas-phase water, is assigned to a non-hydrogen-bonded OH stretch. The other three peaks are hydrogen-bonded and have been assigned to "liquid-like" and "ice-like" water structures (Table 2).

The assignment of a peak at 3117 cm^{-1} is new and arises directly from the requirement that the phase of the imaginary portion of $\chi^{(2)}$ must change its sign near 3200 cm^{-1}. This low-frequency peak should almost certainly be assigned to an ice-like structure. Its frequency is at the lower end of the IR

TABLE 1: Force Field Parameters for Water Models

model	type	r_0 (Å)	ε (kcal/mol)	r_1 (Å)	r_2 (Å)	q_1 (e)	q_2 (e)	θ (deg)	φ (deg)
SPC/E	a	1.7767	0.1553	1.0000		0.4238	−0.8476	109.47	
TIP3P	a	1.7683	0.152	0.9572		0.417	−0.834	104.52	
POL3	a	1.798	0.156	1.0000		0.365	−0.730	109.47	
TIP4P-Ew	b	1.775931	0.16275	0.9572	0.1250	0.52422	−1.04844	104.52	52.26
TIP5P	c	1.7510	0.160	0.9572	0.70	0.241	−0.241	104.52	109.47
mTIP5P	c	1.7510	0.160	0.850	0.850	0.241	−0.241	109.47	109.47

SCHEME 2: Cuboid Water Slab and the Definitions of the Orientations of the O−H Bond, O-Lp,[a] and the Water Dipole

[a] Lp: lone-pair electrons.
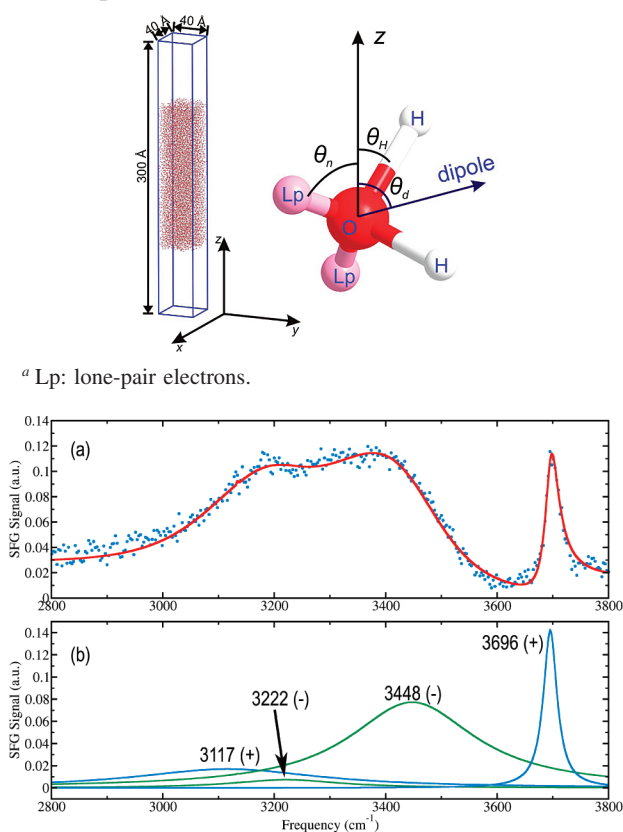
Figure 1. (a) VSFS of the air/water interface with the ssp polarization combination. The open circles and the red solid line are experimental data and the overall fit to the data, respectively. (b) Four component peaks are directly derived from the fit in part a. Peaks with postive signs are in blue and negative signs are in green.

absorption band for ice. Moreover, the highest peak in the Raman spectrum for ice is at 3085 cm^{-1}, which is much lower than in the IR.[29–31] For a molecular vibration to be observable in VSFS, it has to be both IR and Raman active.[4] Because there are multiple absorption peaks in the IR and Raman spectra of ice as well as many other solid forms of water,[29,30,32,33] it is not surprising that there might be multiple ice-like peaks found in the VSFS spectrum.

VSFS not only reports information on oscillator frequency and strength, but also on the net orientation of the associated transition dipole moment.[1,4–6] For OH vibrations, the orientation

TABLE 2: Fitting Parameters and Peak Assignments for the Spectrum in Figure 1

frequency (cm^{-1})	strength	width (cm^{-1})	assignment
3696	+5.6	15	gas-like
3448	−38.2	137	liquid-like
3222	−10.0	117	ice-like
3117	+26.4	202	ice-like

of the transition dipole is along the direction of the OH bond. Absolute orientation information, oscillator strength data, as well as peak width values for each of the four resonances are provided in Table 2. The 3696 cm^{-1} peak carries a positive sign,"+", and it is assumed to face up into the gas phase. Therefore, the 3116 cm^{-1} peak should have the same orientation. On the other hand, both the 3448 and 3222 cm^{-1} peaks carry a negative sign, "−", and therefore, the corresponding OH moieties should point in the opposite direction, toward the bulk liquid.

MD Simulations

Density Profile. In a first set of simulation studies, results were obtained using the SPC/E model. The density of water along the z-direction is shown in Figure 2. As can be seen from the figure, the thickness of the air/liquid interface is about 4 Å when the interface is defined as the region between 5% and 95% of the bulk liquid density. Moreover, the density profile can be fit to a hyperbolic tangent function:

$$\rho(z) = a\{1 + \tanh[b(z - c)]\} \tag{3}$$

whereby, $a = 0.493$ g/cm,[3] $b = 0.5735$ Å^{-1}, $c = 71.296$ Å. It should be noted that the value of c denotes the position of the Gibbs dividing surface.[2]
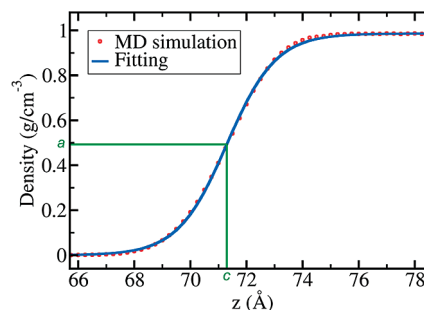

Figure 2. Density profile along the z-direction of the water slab.

Structure of Water at the Aqueous/Air Interface

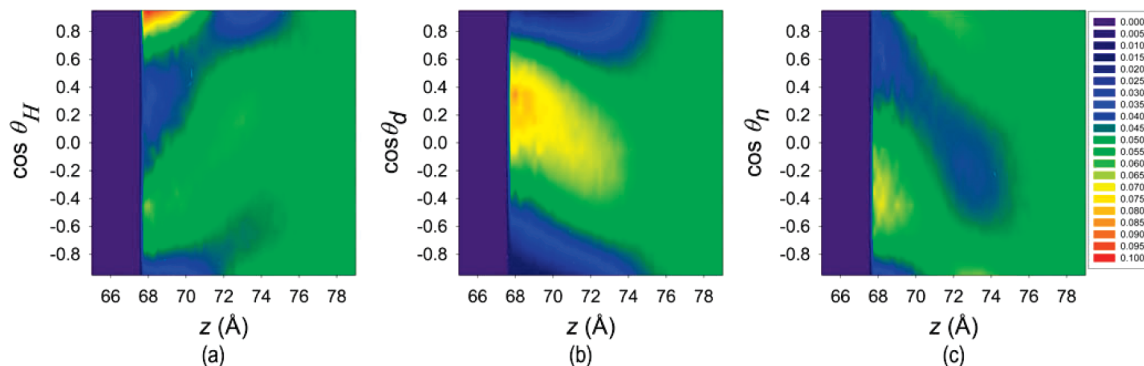*J. Phys. Chem. B, Vol. 113, No. 34, 2009* **11675**

Figure 3. Probability distributions as a function of depth (*z*-axis) for the orientation of (a) the OH groups, (b) the water dipoles, and (c) O-Lp.
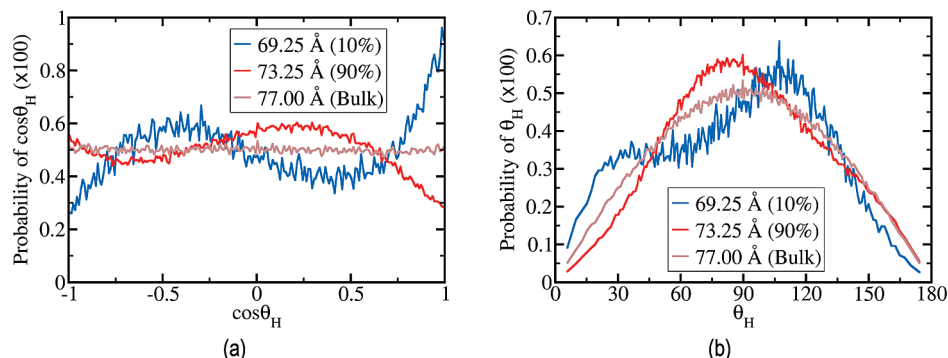

Figure 4. $P(\cos \theta_H)$ and $P(\theta_H)$ at three typical depths corresponding to the different interfacial layers.

Layered Structures at the Air/Water Interface and Comparison to Ice Surfaces. Next, we analyze the water orientation at various depths into the liquid bulk. Figure 3 reports the calculated distribution functions for $\cos \theta_H$, $\cos \theta_d$, and $\cos \theta_n$, respectively, with the angles defined in Scheme 2. It is clear from Figure 3a that the interface has a partially ordered structure, as judged from the uneven distribution of $P(\cos \theta_H)$. Furthermore, the $P(\cos \theta_H)$ values are significantly different at different depths. According to the distribution plot for $\cos \theta_H$, one can divide the interface into two distinct layers corresponding to the range from 68 to 71 Å (5−50% of the bulk density) and from 71 to 75 Å (50−95% of the bulk density). The distribution functions $P(\cos \theta_d)$ and $P(\cos \theta_n)$ also show the partially ordered structure at the interface. For example, the water dipoles near the interface tend to be perpendicular to the surface normal, which is consistent with previous simulation results.[2]

The distribution function for θ_H is shown in Figure 4 at three different depths, representing bulk water and the two interfacial layers. It can be seen from Figures 3 and 4 that the distribution function $P(\cos \theta_H)$ peaks at about 1 and −0.4 in the top layer, which corresponds to water molecules with one OH bond pointing vertically out of the bulk liquid and the other OH bond at ~110°. This second OH, therefore, points slightly downward into the bulk solution. It should be noted that the angle between the two bonds is consistent with the restriction of the intrinsic bond angle (109.47°) for SPC/E water. In the second layer, the distribution function for $P(\cos \theta_H)$ reaches minima near −0.4 and at 1.0 with one of the two OH bonds pointing into the bulk.

The layered structure at the air/water interface can be compared to that of the (1000) crystal face of ice I_h, as suggested previously by Shen and co-workers.[1,7] Two types of water molecules are present in the top layer of an "ideal" ice surface. These are labeled DDA and DAA in Figure 5. The first has a dangling OH bond pointing vertically out of the crystal, while the other has a lone pair pointing upward. Here, DDA refers to the fact that this type of water has three hydrogen bonds: two
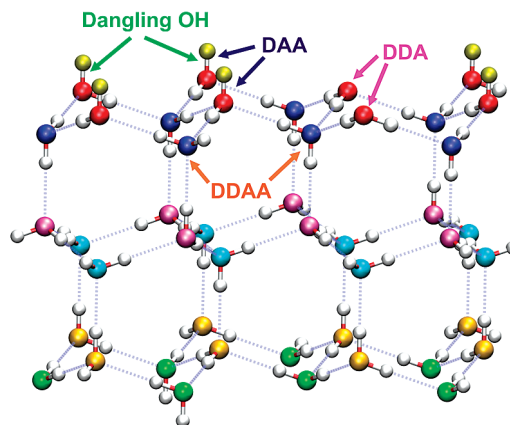

Figure 5. Cartoon of ice (I_h) surface. All water oxygens at the same level are shown in the same color.

donors (D) and one acceptor (A). It should be noted that at the air/water interface, neither DDA nor DAA may form all three hydrogen bonds as they do at an ice surface because of the lower density. Interfacial water molecules with one OH pointing upward are nevertheless denoted as DDA, because such molecules can potentially form three hydrogen bonds.

The orientation of water molecules at the ice surface and the air/water interface is quite similar, although the latter is found to have a broader distribution by simulation. It should be noted that at least part of this broadening is caused by a capillary wave effect,[34,35] which is the result of the box size that was employed in the present MD simulations (40 × 40 × 300 Å³). The structural similarity between the air/water interface and the ice surface can also be seen in the second layer (centered at a water density of ~50%, Figure 3b). In both systems the plane of the water molecules tends to line up with the interface and one OH bond points into the bulk. The key difference between the ice surface and the air/water interface is again in their density

profiles. When the polar angle is taken into account, the water molecules in the top layer of the liquid show a maximum probability for pointing out of the bulk at an angle of ~30° with respect to the surface normal (Figure 4b, the blue trace shows a local maximum near 30°). This result is in agreement with a multiple-configuration VSFS study by Wang and co-workers[36,37] that showed that the average tilt angle is ~30°. In this sense, the air/water interface is only similar to the (1000) ice surface locally and only in one dimension (parallel to the surface normal), and each local structure is tilted at a unique angle. Therefore, the water/air interface cannot be considered to have an ice layer. Another major difference between the ideal ice surface and the air/water interface simulated using the SPC/E model involves a large depletion of DAA waters compared with DDA. This can be easily seen from the difference in the distribution functions $P(\cos \theta_H)$ and $P(\cos \theta_n)$, which will be discussed below.

Assignment of the VSFS Peaks

Standard Model. As noted above, there are a total of four peaks in the VSFS spectrum (Figure 1 and Table 1). Water molecules that have their molecular planes parallel to the interface should contribute little to this spectrum. This is because a molecular vibration, to a first-order approximation, must be preferentially oriented along the surface normal to be active for a system such as the air/water interface, which is isotropic in plane.[4] Therefore, the four peaks in Figure 1 should be produced by OH vibrations tilted at least somewhat upward or downward. As such, the following assignments can be made in accordance with Scheme 1: The 3696 cm^{-1} peak arises from the free OH pointing away from the bulk in agreement with past assignments. The 3117 cm^{-1} peak has the same sign as the 3696 cm^{-1} peak. This peak should, therefore, correspond to water molecules in the second layer that have their OH groups pointing upward to hydrogen bond with water molecules in the first layer. On the other hand, the hydrogen-bonded OH groups in the first layer point downward and, therefore, should give rise to a feature with a sign opposite to the 3696 cm^{-1} peak. The 3222 cm^{-1} feature is, therefore, assigned to this species. The OH groups pointing downward in the first layer (3222 cm^{-1} feature) and the OH groups pointing upward in the second layer (3117 cm^{-1}) are very like the top layers of ice (Figure 5). These OH groups face each other, but their oscillator strengths do not completely cancel one another out. This is the case in part because the number density of water molecules in the second layer is greater than that in the first. Since there is a depletion of DAA compared to DDA in the first layer, there are more hydrogen acceptors available from the first layer than donors. As a result, one would expect to observe more ice-like OH groups from the second layer (pointing up) than from the first layer (pointing down). Thus, an overall peak with a positive sign should prevail if the frequencies from these two layers were identical. Indeed, the oscillator strength of the 3117 cm^{-1} peak is greater than the one at 3222 cm^{-1}. However, the chemical environments from these two layers are somewhat different. Specifically, the 3222 cm^{-1} feature arises from water molecules in which one of the OH moieties is not hydrogen bonded, while this is not true for the 3117 cm^{-1} species. Therefore, the frequencies from these two species should not be identical and perfect cancellation should not be observed.

Finally, the 3448 cm^{-1} peak is assigned to OH groups pointing downward from the second layer. The fact that this resonance has a sign that is opposite to the 3696 cm^{-1} peak is consistent with this assignment. These OH groups are hydrogen bonded to water molecules in the layer beneath them, which is much more disordered than water molecules in the first two layers. Therefore, one would expect these OH moieties to possess a liquid-like frequency. Here, we note that this layer has the greatest oscillator strength, which is consistent with the perpendicular orientation of these OH moieties as well as the relatively high number density of molecules present in this layer.

A distinction between the peak assignments presented here and previous ones is that we assume that OH groups pointing in the same direction in each layer have an indistinguishable VSFS spectrum, while water species at different depths are distinguishable because of environmental differences and/or differences in bonding. Also, it should be pointed out that the assignments of the 3448 and 3222 cm^{-1} peaks could in principle be interchanged if only the signs were considered. However, the oscillator strength from the 3448 cm^{-1} peak is significantly stronger than the oscillator strength from the 3222 cm^{-1} peak. Moreover, it is more than 200 cm^{-1} blue-shifted with respect to the 3222 cm^{-1} peak. These facts are consistent with a more liquid-like peak that contains a higher density of oscillators and, hence, originates from deeper within the liquid surface.

Assignments Based upon the Evan's Window Model. A new interpretation for the ~3200 and ~3450 cm^{-1} peaks was recently put forth by Bonn and co-workers.[38] They observed that the two peaks (in O—D stretching region) coalesce upon isotropic dilution. On the basis of this observation, these authors suggested that the dip between the two broad humps is the result of an Evan's window. In other words, a Fermi resonance with water's bending mode splits an extremely broad single OH stretch peak (roughly ranging from 3000 to 3500 cm^{-1}) into two apparently separate features. If this interpretation is correct, an adjustment to the above stated model would be necessary. The 3696 cm^{-1} feature would still arise from the free OH moieties in the first layer. The peak at 3117 cm^{-1}, however, would need to be assigned as the only ice-like peak. This could be the case if the OH oscillators in the first and second layers, which point toward one another, lead to maximum cancelation. The 3222 and 3448 cm^{-1} resonances would then be part of the same very broad "water-like" peak with its true resonance occurring at an intermediate frequency. It should be noted, however, that Shen and co-workers offered an alternative interpretation of the observation of the apparently single feature upon isotropic dilution.[39] On the basis of their phase-sensitive VSFS results, they suggested that there are still two (or multiple) peaks instead of one. If this interpretation is correct, no adjustment would be necessary to the model presented here.

Discussion

Hydrogen Bonding and Charge Burial Determine Water Structure in the First Layer. Simulations using most water models involving point charges (including a polarizable model) yield a water orientation consistent with VSFS measurements in that a single dangling OH bond points out of the bulk liquid. This orientation is postulated to be the result of two factors: (1) maximization of the number of hydrogen bonds per molecule and (2) a tendency to bury the greatest amount of partial charge into the liquid phase. In order to form the maximum number of hydrogen bonds, an interfacial water molecule tends to orient as many hydrogen-bond-forming sites as possible into the liquid below. The roughly tetrahedral arrangement of the hydrogen-bond-forming sites thus results in a single site, one hydrogen or lone pair, pointing away from the bulk liquid. This tendency gives rise to probability distribution functions for θ_H and θ_n, which correspond to DDA and DAA species, respectively

Structure of Water at the Aqueous/Air Interface

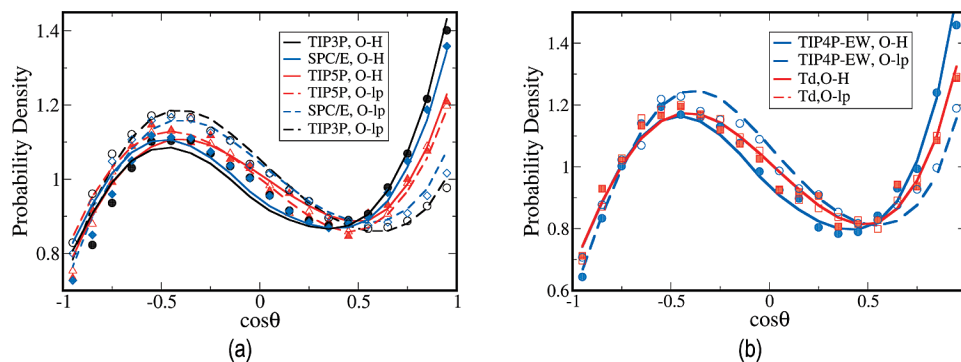*J. Phys. Chem. B, Vol. 113, No. 34, 2009* **11677**

Figure 6. The distribution functions for the angles between surface normal and the OH bond or O-Lp vector calculated using different water models. The data represented by symbols were obtained from molecular dynamics simulations, and the lines are obtained using the simple theory described in the text.

(Figure 4). As shown in Figure 5, such distributions were indeed observed for both θ_H and θ_n; however, the former is much more pronounced than the latter. Moreover, the extent of DDA depletion is strongly dependent on the model employed in the simulations. Such model-dependent differences arise from the assumed charge distribution as well as the propensity of each model to expose less charge at the interface.

In the point charge model for gas-phase water molecules, a partial positive charge of $+q$ is present on each hydrogen and a negative charge of $-2q$ is centered on the oxygen. This is essentially the picture provided by the SPC/E model and either θ_H or θ_n must be zero. Two effective potentials can be defined as a function of water orientation, F_t and F_c, to describe the maximization of hydrogen-bond formation and the minimization of charge exposure, respectively. In this model, F_t will take on a minimum value when one of the hydrogen-bonding sites points out of the bulk liquid, as this will maximize the formation of hydrogen bonds at the interface. On the other hand, F_c measures the amount of charge that is exposed and takes on a minimum value when the least charge is exposed. For simplicity, F_t can be written in the following Gaussian-type form

$$F_t = \omega_H \sum_{i=1}^{4} \exp(-(\cos \theta_i - 1)^2/2\sigma_H^2) \qquad (4)$$

where θ_i is the angle between the vector connecting the oxygen to the ith hydrogen-bonding site and the surface normal. ω_H and σ_H are parameters describing the strength and the width of this potential, respectively.

F_c describes the energy penalty due to the exposure of charges to a low charge density region (i.e., a vacuum). This function can be written as

$$F_c = \omega_n \sum_{i=1}^{4} (\min(z_i) - z_i)|q_i| \qquad (5)$$

In eq 5, z_i is the depth of the ith hydrogen-bonding (charge) site with respect to the topmost point charge, $\min(z_i)$. On the other hand, $|q_i|$ is the absolute value of the partial charge at this site. The smaller the value of F_c, the less charge is exposed to the gas phase. For simplicity, it is assumed in eq 5 that the decrease in energy due to the burial of a partial charge into the bulk is linearly dependent on z.

A Monte Carlo simulation was performed to sample the orientation of water molecules using various models and the

TABLE 3: Parameters Used in Eqs 4 and 5

	ω_H (kT)	σ_H^2	ω_n (kT)
SPC/E	2.7	0.75	0.19
TIP3P	2.7	0.75	0.19
TIP5P	2.7	0.75	0.19
TIP4P-Ew	2.7	0.50	0.19
mTIP5P(T$_d$)	2.2	0.75	0.19

energy function, $F_t + F_c$, so that the equilibrated distribution follows $\exp[-(F_t + F_c)/kT]$, with k being Boltzmann's constant and T being the temperature. Strictly speaking, such a model should also take into account the roughness of the surface. Namely, water molecules at the same depth (or average density) have different local environments (e.g., density and/or hydrogen bonding). It should also be noted that the force parameters in eqs 4 and 5 are depth-dependent and sensitive to the local hydrogen-bonding environment. Therefore, to circumvent these complexities, we focus only on the top water layer in Scheme 1. Therefore, the only water molecules that are taken into account are those for which the liquid density is 10% or less of the bulk liquid value.

For all the models, the parameter that describes the energy penalty due to exposed charge, ω_n, takes on the same value (eq 5). Somewhat different values of ω_H and σ_H^2 were obtained for different water models due to their different tendencies for forming hydrogen bonds through a simple fitting for the distribution of θ_H. These parameters are employed for calculating the distribution of θ_n. The calculated results using expressions 4 and 5 are compared with the MD simulation results for each individual water model in Figure 6. The agreement between the all atom simulations and the simple theoretical model was satisfactory. All parameters employed are provided in Table 3.

Focusing first on Figure 6a, one sees that the distribution $P(\cos \theta_H = 1)$ has the following order: SPC/E > TIP3P > TIP5P. On the other hand, the distribution $P(\cos \theta_n = 1)$ follows the opposite order: TIP5P > TIP3P > SPC/E. The differences between the SPC/E and TIP3P models are quite small and may be understood as follows: The SPC/E and TIP3P models have similar charge distributions with two positive partial charges on each of the hydrogen atoms and a negative charge on the oxygen atom. Since the magnitude of negative charge is twice that of each of the positive charges, the exposure of one of the positive charges is energetically more favorable than the exposure of the negative charge. This leads to a much higher probability for an OH bond to point upward compared to a lone pair. Furthermore, the charges for the SPC/E model are larger than those employed in the TIP3P model. Thus, the difference between an OH and a lone pair pointing upward is larger in the

former case. For the TIP5P model, the positive and negative charges have similar distances to the oxygen atom. As a result, the probabilities for an OH and a lone pair pointing out of the bulk liquid are very close.

Given that the charge distribution determines the relative probability of an OH vs a lone pair pointing out the surface, an artificially constructed water model, which has a tetrahedral arrangement of point charges, would yield the same distribution function for cos θ_H and cos θ_n. As seen in Figure 6b, this is indeed the case. On the other hand, the TIP4P-Ew model has an uneven charge distribution and shows different distribution functions for the OH bonds and for the lone pairs, similar to TIP3P and SPC/E. The difference between TIP4P-Ew and the other models is that the peaks at angle zero are sharper in the former case and thus the potential has a smaller width. This difference is a result of the narrower distribution of the H−O−H angles when tetrahedral-like structure is formed in the TIP4P-Ew model. It was shown that with the increase of the angle θ (thus the model becomes more TIP4P like; see Table 1), the SPC/E model forms hydrogen bonds with a narrower angle distribution, resulting in a more tetrahedral-like structure.[40]

On the basis of the simulations performed using the water models described above, we conclude that the orientation of water in the top layer can be understood qualitatively in terms of energetic considerations. Namely, to maximize hydrogen-bond formation as well as the burial of partial charge, water molecules orient with a single OH pointing out of the surface. Other effects might influence this process, but they were not considered in these models. Such effects include dipole−dipole interactions and the depth dependence of charge burial. These effects are probably of secondary importance. Nonetheless, we should emphasize that the simple treatment described above is only appropriate for water molecules that are in the top layer, for which hydrogen bonds can be formed only with water molecules deeper into the bulk.

Choice of Water Models. Several water models with different charge distributions were employed in the present study. These models all yield partially structured interfaces in the density range of ∼5−95%. Moreover, all simulated results partly resemble the surface of ice. However, strong model-dependent distribution functions were observed for the orientation of water at the air/water interface. Indeed, by simply changing the charge distributions for a given water model, drastically different results for interfacial water structure could be obtained. For example, the further a partial charge was placed away from the oxygen atom, the more likely the vector connecting it to the oxygen atom was found to be pointing into the bulk. Therefore, the comparison of simulation results with experiments depends heavily on the model employed. Quantum calculations show that the partial charge on each hydrogen atom of a gas phase water molecule is about +0.58e and the oxygen atom carries a charge of approximately −1.16e, making SPC/E, TIP3P, and TIP4P-Ew the most reasonable models for gas-phase water molecules. In the bulk liquid, however, a shift of negative charge from the oxygen atoms to the tetrahedral positions is expected and a model similar to TIP5P may provide a better description.

At the interface, the amount of charge redistribution that occurs should fall in between the gas phase and bulk liquid limits. Therefore, three charge site models may be the most appropriate route for simulating interfacial water structure. The fact that the SPC/E model was shown to yield results consistent with VSFS measurements is consistent with this notion.[36] Specifically, SPC/E predicts a peak distribution of OH orienta-

tions at about 30°, which is in agreement with spectroscopic observations.[36] As such, one might expect that a complete description of the combined bulk and interfacial water regimes would require either polarizable models or a full quantum treatment. Indeed, the charge distributions of these two regions are undoubtedly quite different. On the other hand, our simulations using one of the polarizable models, POL3, yielded results that are very similar to the SPC/E and TIP3P models.

Water Structure in the Second Layer and Beyond. The partial ordering of water in the second layer can be understood in the same terms as the ordering in the first. In fact, the same factors should be at play. Namely, a balance between the maximization of hydrogen bonding and a minimization of exposed charge should help dictate the water structure. The density of water molecules is higher in the second layer than the first. Therefore, the effects of charge burial should be less pronounced. With this being the case, the main factor determining water structure should be maximization of hydrogen-bonding interactions. In particular, hydrogen bonding to the top layer will be of great importance. Since hydrogen bonds are directional, the uneven $P(\cos \theta_H)$ distribution in the first layer will induce an uneven $P(\cos \theta_H)$ distribution in the second one. Upon the basis of both simulations and VSFS data, this clearly appears to be the case.

The next question is the extent to which ordering can be observed beyond the second layer. As already noted above, the degree of alignment observed in the present simulations was far less pronounced in the second layer compared with the first. Moreover, thermal fluctuations will counteract the ordering effects of one water layer upon the next. Figure 4 plots the $P(\cos \theta_H)$ distribution at a depth of 77 Å. As can be seen, the distribution is flat within the error bars, which is consistent with the notion that the third layer possesses little if any interfacial ordering effects.

Peak Widths of the Ice-Like Features. The next topic we wish to address is the rather broad peak widths that were found for the two ice-like features, particularly for the 3117 cm^{-1} resonance. Curiously, these peaks are broader than the water-like feature at 3448 cm^{-1}. Such widths cannot be explained by the nature of the hydrogen bonding and vibrational coupling alone. Instead, this finding is likely the result of structural inhomogeneity at the air/water interface. The interface, though ice-like, is much more diffuse and rougher than a corresponding ice crystal would be. Moreover, it is well-known that water can adopt various polymorphs.[29,30,32,33] Most of these structures show an OH stretching band near 3200 cm^{-1} in the IR and near 3100 cm^{-1} in the Raman, similar to the ice I_h crystal, but much more diffuse and complicated. Therefore, there should be multiple ice-like species contributing to the 3117 and 3222 cm^{-1} peaks, despite the fact that only a single peak has been used to fit both of them. Indeed, Shen and co-workers have already suggested that this region of the spectrum should be attributed to a "continuum" of frequencies.[7]

Delocalization of Hydrogen Bonds. Very recently, using a combined quantum mechanical/classical mechanical approach, several groups studied in great detail the vibrational spectroscopy of bulk water, which showed that the OH-stretch vibrational excitations are delocalized over many molecules (∼12 chromophores) and possess an excitonic nature.[41–45] A detailed and careful analysis on how vibrational excitation is delocalized at the interfaces,[41] where the distribution of water molecules is asymmetric along the surface normal and the water density is low, is needed. If the same excitonic nature is found for interfacial water molecules, one should expect that the collective

Structure of Water at the Aqueous/Air Interface

J. Phys. Chem. B, Vol. 113, No. 34, 2009 **11679**

nature of the vibrational models to have a significant effect on the transition frequencies of the differently hydrogen-bonded and oriented water molecules, which contribute in the broad 3100−3600 cm^{-1} range.[43,46] However, the identification of three spectral regions with alternating phases possibly indicates that the mixing of the vibrational modes does not override the signatures of water molecules of different orientations with respect to the interface. Therefore, in this paper, we provide a first-order approximation for the connection between the phase of the spectrum and the averaged molecular orientation at the air/water interfaces. In fact, the delocalized nature of the vibrational coupling between a fairly large number of oscillators indicates that the vibrational frequencies of water species at the interface are strongly influenced by partially ordered water molecules with unsaturated hydrogen bonds (e.g., Figure 3; in the top layer the OH moiety prefers to point out of the bulk water). The strong coupling (both intra- and intermolecular) among the chromophores and the preferred orientations of the chromophores at and near the interface would therefore affect the vibrational excitation frequencies detected with surface-specific techniques such as VSFS. Finally, we should note that the present assignments will need to be subjected to further theoretical and experimental tests.

References and Notes

(1) Shen, Y. R.; Ostroverkhov, V. *Chem. Rev.* **2006**, *106*, 1140.

(2) Lee, C. Y.; Mccammon, J. A.; Rossky, P. J. *J. Chem. Phys.* **1984**, *80*, 4448.

(3) Morita, A.; Hynes, J. T. *Chem. Phys.* **2000**, *258*, 371.

(4) Shen, Y. R. *The Principles of Nonlinear Optics*; Wiley: New York, 1984.

(5) Richmond, G. L. *Chem. Rev.* **2002**, *102*, 2693.

(6) Gopalakrishnan, S.; Liu, D. F.; Allen, H. C.; Kuo, M.; Shultz, M. J. *Chem. Rev.* **2006**, *106*, 1155.

(7) Ji, N.; Ostroverkhov, V.; Tian, C. S.; Shen, Y. R. *Phys. Rev. Lett.* **2008**, *1*, 096102.

(8) Brown, E. C.; Mucha, M.; Jungwirth, P.; Tobias, D. J. *J. Phys. Chem. B* **2005**, *109*, 7934.

(9) Ishiyama, T.; Morita, A. *Chem. Phys. Lett.* **2006**, *431*, 78.

(10) Wilson, M. A.; Pohorille, A.; Pratt, L. R. *J. Phys. Chem.* **1987**, *91*, 4873.

(11) Kuo, I. F. W.; Mundy, C. J.; Eggimann, B. L.; McGrath, M. J.; Siepmann, J. I.; Chen, B.; Vieceli, J.; Tobias, D. J. *J. Phys. Chem. B* **2006**, *110*, 3738.

(12) Townsend, R. M.; Rice, S. A. *J. Chem. Phys.* **1991**, *94*, 2207.

(13) Matsumoto, M.; Kataoka, Y. *J. Chem. Phys.* **1988**, *88*, 3233.

(14) Walker, D. S.; Hore, D. K.; Richmond, G. L. *J. Phys. Chem. B* **2006**, *110*, 20451.

(15) Kuo, I. F. W.; Mundy, C. J. *Science* **2004**, *303*, 658.

(16) Wilson, K. R.; Rude, B. S.; Catalano, T.; Schaller, R. D.; Tobin, J. G.; Co, D. T.; Saykally, R. J. *J. Phys. Chem. B* **2001**, *105*, 3346.

(17) Wilson, K. R.; Cavalleri, M.; Rude, B. S.; Schaller, R. D.; Nilsson, A.; Pettersson, L. G. M.; Goldman, N.; Catalano, T.; Bozek, J. D.; Saykally, R. J. *J. Phys.: Condens. Matter* **2002**, *14*, L221.

(18) Cappa, C. D.; Smith, J. D.; Wilson, K. R.; Saykally, R. J. *J. Phys.: Condens. Matter* **2008**, *20*, 205105.

(19) Berendsen, H. J. C.; Grigera, J. R.; Straatsma, T. P. *J. Phys. Chem.* **1987**, *91*, 6269.

(20) Jorgensen, W. L.; Chandrasekhar, J.; Madura, J. D.; Impey, R. W.; Klein, M. L. *J. Chem. Phys.* **1983**, *79*, 926.

(21) Mahoney, M. W.; Jorgensen, W. L. *J. Chem. Phys.* **2000**, *112*, 8910.

(22) Horn, H. W.; Swope, W. C.; Pitera, J. W.; Madura, J. D.; Dick, T. J.; Hura, G. L.; Head-Gordon, T. *J. Chem. Phys.* **2004**, *120*, 9665.

(23) Caldwell, J. W.; Kollman, P. A. *J. Phys. Chem.* **1995**, *99*, 6208.

(24) Case, D. A.; Darden, T. A.; Cheatham, I., T.E.; Simmerling, C. L.; Wang, J.; Duke, R. E.; Luo, R.; Merz, K. M.; Pearlman, D. A.; Crowley, M.; Walker, R. C.; Zhang, W.; Wang, B.; Hayik, S.; Roitberg, A.; Seabra, G.; Wong, K. F.; Paesani, F.; Wu, X.; Brozell, S.; Tsui, V.; Gohlke, H.; Yang, L.; Tan, C.; Mongan, J.; Hornak, V.; Cui, G.; Beroza, P.; Mathews, D. H.; Schafmeister, C.; Ross, W. S.; Kollman, P. A. *AMBER 9*; University of California: San Francisco, 2006.

(25) Ryckaert, J. P.; Ciccotti, G.; Berendsen, H. J. C. *J. Comput. Phys.* **1977**, *23*, 327.

(26) Darden, T.; York, D.; Pedersen, L. *J. Chem. Phys.* **1993**, *98*, 10089.

(27) Chen, X.; Yang, T.; Kataoka, S.; Cremer, P. S. *J. Am. Chem. Soc.* **2007**, *129*, 12272.

(28) Chen, X.; Sagle, L. B.; Cremer, P. S. *J. Am. Chem. Soc.* **2007**, *129*, 15104.

(29) Eisenberg, D. W. K. *The Structure and Properties of Water*; Oxford University Press: New York, 1969.

(30) Ockman, N. *Adv. Phys.* **1958**, *7*, 199.

(31) Buch, V.; Tarbuck, T.; Richmond, G. L.; Groenzin, H.; Li, I.; Shultz, M. J. *J. Chem. Phys.* **2007**, *127*, 204710.

(32) Sivakumar, T. C.; Rice, S. A.; Sceats, M. G. *J. Chem. Phys.* **1978**, *69*, 3468.

(33) Bergren, M. S.; Schuh, D.; Sceats, M. G.; Rice, S. A. *J. Chem. Phys.* **1978**, *69*, 3477.

(34) Sides, S. W.; Grest, G. S.; Lacasse, M. D. *Phys. Rev. E: Stat. Phys., Plasmas, Fluids, Relat. Interdiscip. Top.* **1999**, *60*, 6708.

(35) Ismail, A. E.; Grest, G. S.; Stevens, M. J. *J. Chem. Phys.* **2006**, *125*, 014702.

(36) Gan, W.; Wu, D.; Zhang, Z.; Feng, R. R.; Wang, H. F. *J. Chem. Phys.* **2006**, *124*, 114705.

(37) Gan, W.; Wu, D.; Zhang, Z.; Guo, Y.; Wang, H. F. *Chin. J. Chem. Phys.* **2006**, *19*, 20.

(38) Sovago, M.; Campen, R. K.; Wurpel, G. W. H.; Muller, M.; Bakker, H. J.; Bonn, M. *Phys. Rev. Lett.* **2008**, *100*, 173901.

(39) Tian, C. S.; Shen, Y. R. *J. Am. Chem. Soc.* **2009**, *131*, 2790.

(40) Chatterjee, S.; Debenedetti, P. G.; Stillinger, F. H.; Lynden-Bell, R. M. *J. Chem. Phys.* **2008**, *128*, 124511.

(41) Auer, B. M.; Skinner, J. L. *J. Chem. Phys.* **2008**, *128*, 224511/1.

(42) Auer, B. M.; Skinner, J. L. *Chem. Phys. Lett.* **2009**, *470*, 13.

(43) Noah-Vanhoucke, J.; Smith, J. D.; Geissler, P. L. *J. Phys. Chem. B* **2009**, *113*, 4065.

(44) Smith, J. D.; Cappa, C. D.; Wilson, K. R.; Cohen, R. C.; Geissler, P. L.; Saykally, R. J. *Proc. Natl. Acad. Sci. U.S.A.* **2005**, *102*, 14171.

(45) Smith, J. D.; Saykally, R. J.; Geissler, P. L. *J. Am. Chem. Soc.* **2007**, *129*, 13847.

(46) Auer, B. M.; Skinner, J. L. *J. Chem. Phys.* **2008**, *129*, 214705/1.